Promoting interfacial charge transfer by B/N co-doping enable efficient ORR catalysis of carbon encapsulating Fe_2N

Zhi Xie [a], Qiaoling Li [a,b], Xingkai Peng [a], Xuewei Wang [a], Lingli Guo [a], Xinghua Zhang [a], Zunming Lu [a], Xiaojing Yang [a], Xiaofei Yu [a], Lanlan Li [a,*]

[a] School of Materials Science and Engineering, Hebei University of Technology, Tianjin 300130, China

[b] School of Materials Science and Engineering, Shandong University of Technology, Zibo 255000, China

*Corresponding Author. *E-mail addresses:* liabc@hebut.edu.cn (L. Li).

Supporting information

Electrochemical Measurements

In the process of cyclic voltammetry (CV) tests, the KOH electrolyte should be bubbled with N_2 or O_2 flow to achieve an oxygen-free or oxygen-saturated environment. For each working electrode test, 20 cycle CVs with a scan rate of 50 mV s^{-1} were accomplished to make it stable. The polarization curves, which were carried out in O_2-saturated 0.1 M KOH solution, were scanned cathodically from 1.1 to 0.2 V at a scan rate of 5 mV s^{-1} with varying rotating speed from 400 rpm to 2025 rpm. The electron transfer number (n) and kinetic current density (J_k) were determined according to the Koutecky–Levich equation:

$$\frac{1}{J} = \frac{1}{J_k} + \frac{1}{J_L} = \frac{1}{J_k} + \frac{1}{B\omega^{1/2}} \quad (1)$$

$$B = 0.20nFC_0D_0^{2/3}\nu^{-1/6} \quad (2)$$

$$J_k = nFkC_0 \quad (3)$$

where J represent the measured electricity density, J_k is the Kinetic density and J_L is the diffusion-limited current density. Besides, F, C_0, D_0, ν, k, and ω are the Faraday constant (96,485 C mol^{-1}), the saturation concentration of O_2 in the 0.1M KOH electrolyte (C_0=1.26×10^{-6} mol cm^{-3}), the O_2 diffusion coefficient (1.9×10^5 cm^2 s^{-1}), the solution viscosity (0.01 cm^2 s^{-1}), the electron-transfer rate constant and the rotation speed of the electrode (rad s^{-1}) respectively.

For the rotating ring disk electrode (RRDE) measurement, the working electrodes were prepared by the same method as the RDE. The peroxide percentage (H_2O_2%, which serves as $2e^-$ pathway selectivity) and electron transfer number (n) were

calculated by the followed equations:

$$H_2O_2\% = 200 \times \frac{I_r/N}{I_d+I_r/N} \quad (4)$$

$$n = 4 \times \frac{I_d}{I_d+I_r/N} \quad (5)$$

Where I_d is the disk current, I_r is the ring current, and N is current collection efficiency of the Pt ring (N = 0.37, provided by the manufacturer).

Supporting Figures

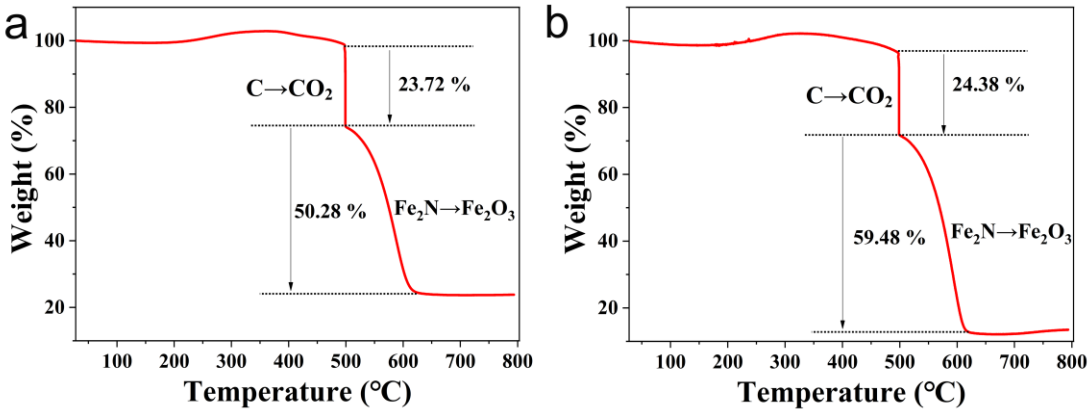

Fig. S1 TGA curves of Fe_2N@BNC-2 (a) and Fe_2N@NC (b) under Air atmosphere from 25 to 800 °C with a heating rate of 10 °C min^{-1}.

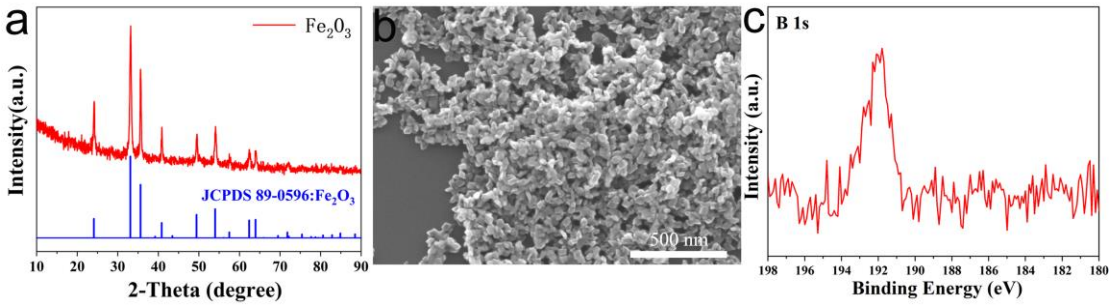

Fig. S2 XRD patterns (a) and SEM image (b) of boron-containing Fe_2O_3 by hydrothermal. (c) B1s XPS spectra of boron-containing Fe_2O_3.

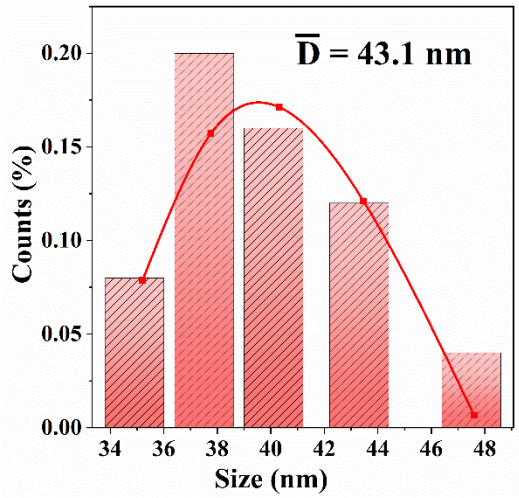

Fig. S3 The size distribution of Fe_2N@BNC-2.

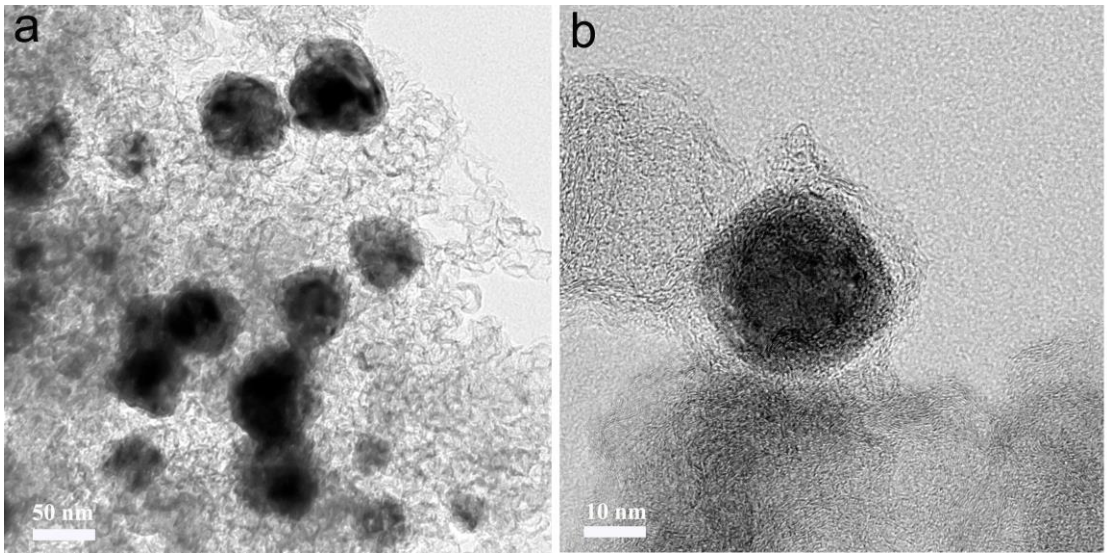

Fig. S4 (a) TEM image of Fe_2N@NC. (b) HRTEM image of Fe_2N@NC

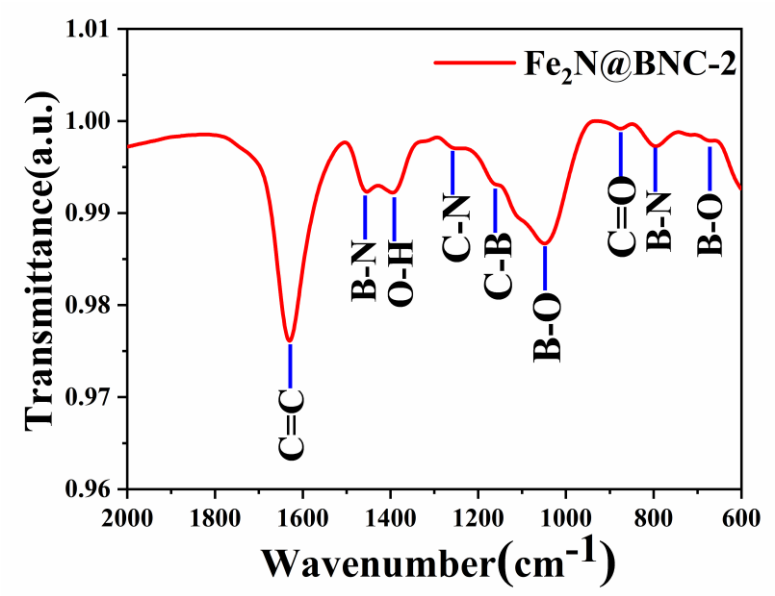

Fig. S5 FTIR spectrum of the Fe_2N@BNC-2.

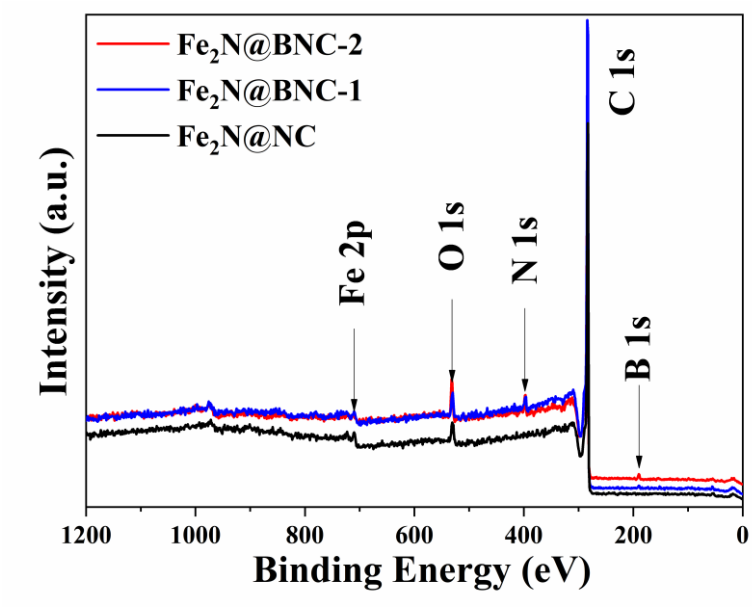

Fig. S6 XPS survey spectra of the various obtained materials.

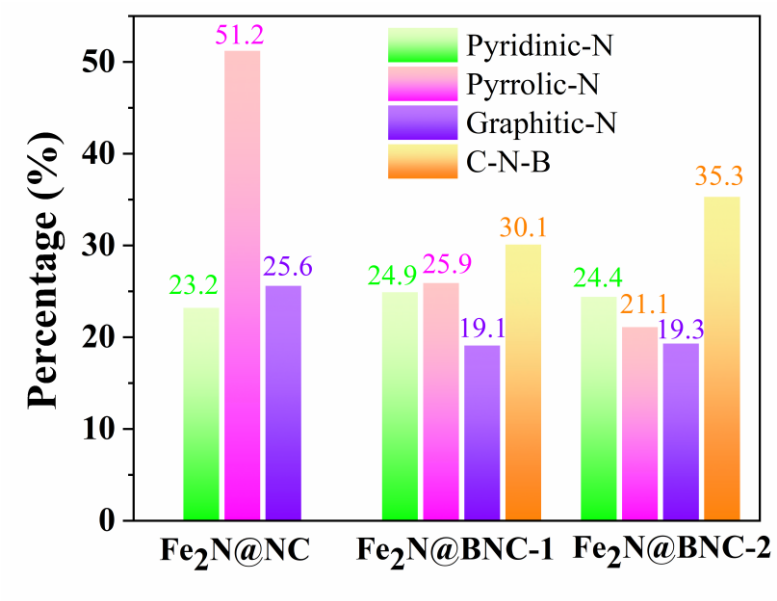

Fig. S7 N bonding configurations and the corresponding contents in Fe_2N@BNC-2, Fe_2N@BNC-1 and Fe_2N@NC.

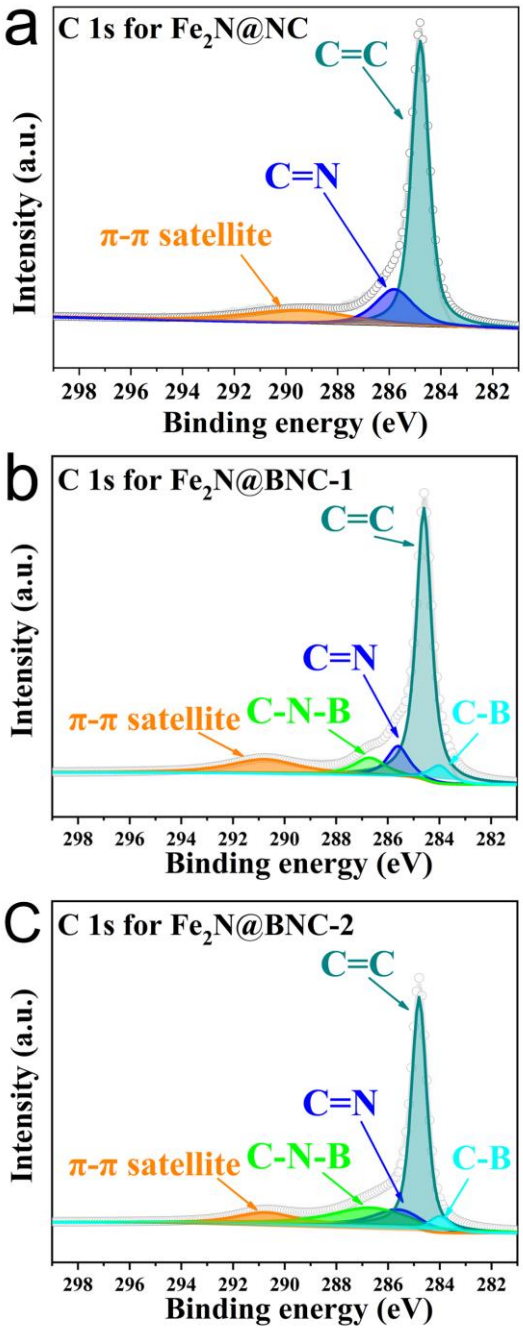

Fig. S8 XPS spectra of C 1s of the Fe_2N@NC (a), Fe_2N@BNC-1 (b) and Fe_2N@BNC-2 (c).

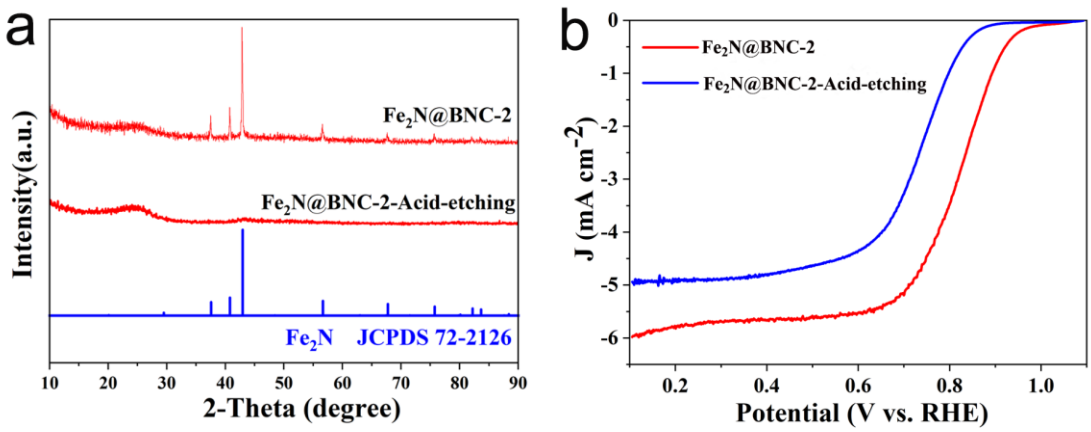

Fig. S9 (a) The XRD of Fe_2N@BNC-2 before and after the removal of Fe_2N. (b) The LSV of Fe_2N@BNC-2 before and after the removal of Fe_2N.

The method is to place the ground sample (Fe_2N@BNC-2) in 2M HCl, pickling at 60°C for 12h. After centrifugation, washed and dried, as-obtained powder was denoted as Fe_2N@BNC-2-acid. As shown in Fig. S9a, the Fe_2N diffraction peak of the Fe_2N@BNC-2 disappeared, only the diffraction peak of the C (002), which indicates that the Fe_2N in the sample was successfully removed after the acid treatment. In Fig. S9b, Fe_2N@NC-2-acid sample exhibits an onset potential of 0.890 V and a half-wave potential of 0.730 V, which is very close to the ORR performance of BNC sample we prepared (E_{onset} = 0.877 V; $E_{1/2}$ = 0.757 V).

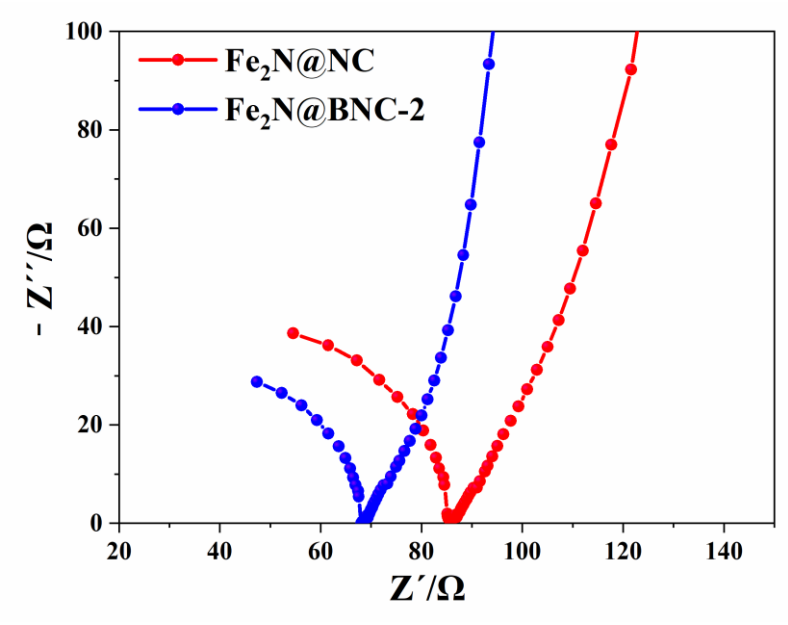

Fig. S10 Electrochemical impedance spectra of Fe_2N@NC and Fe_2N@BNC-2 in oxygen-saturated 0.1 M KOH solution.

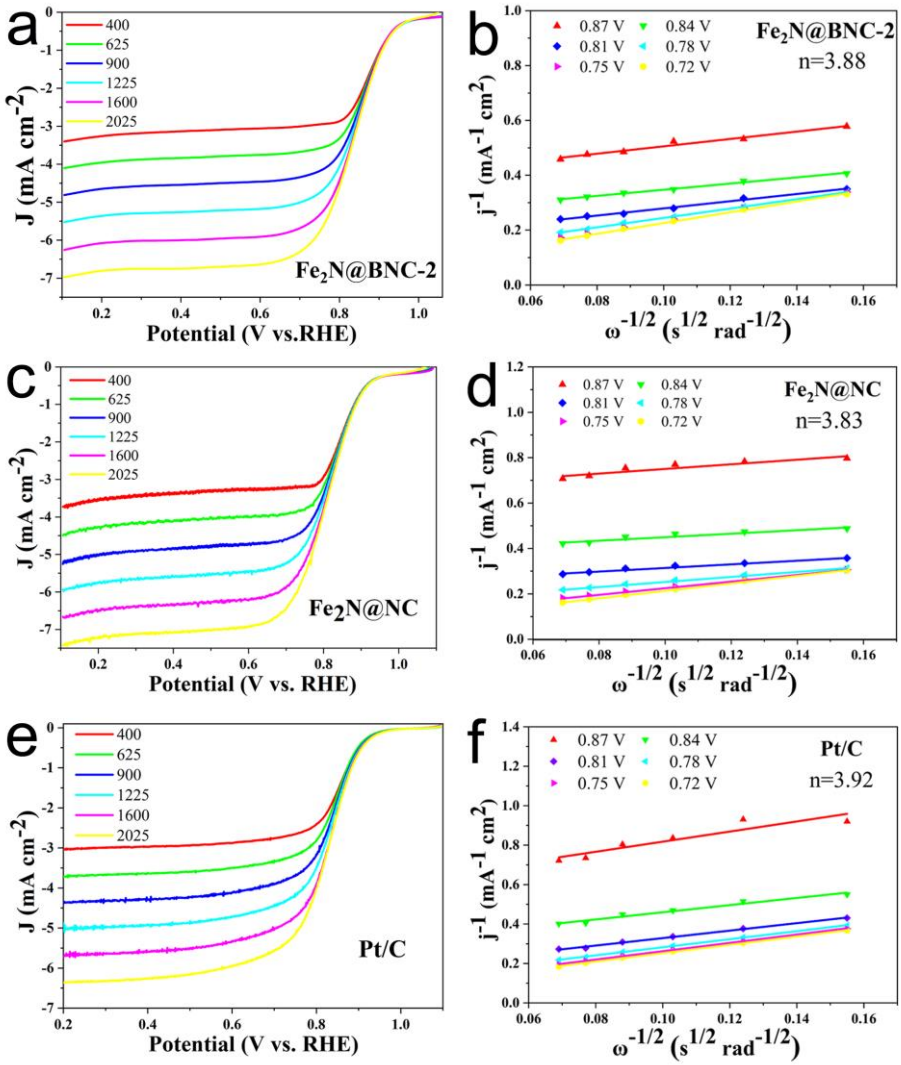

Fig. S11 LSV curves with various rotation rates and corresponding K-L plots (j^{-1} vs. $\omega^{-1/2}$) at different potentials of Fe_2N@BNC-2 (a, b), Fe_2N@NC (c, d) and commercial Pt/C (e, f) in 0.1 M KOH electrolyte.

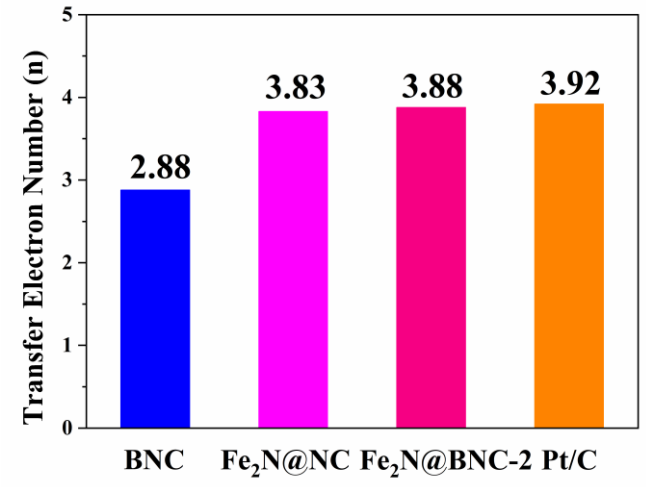

Fig. S12 The K-L formula calculates the transfer electron number (n) for BNC, Fe_2N@NC, Fe_2N@BNC-2, and Pt/C (20 wt%).

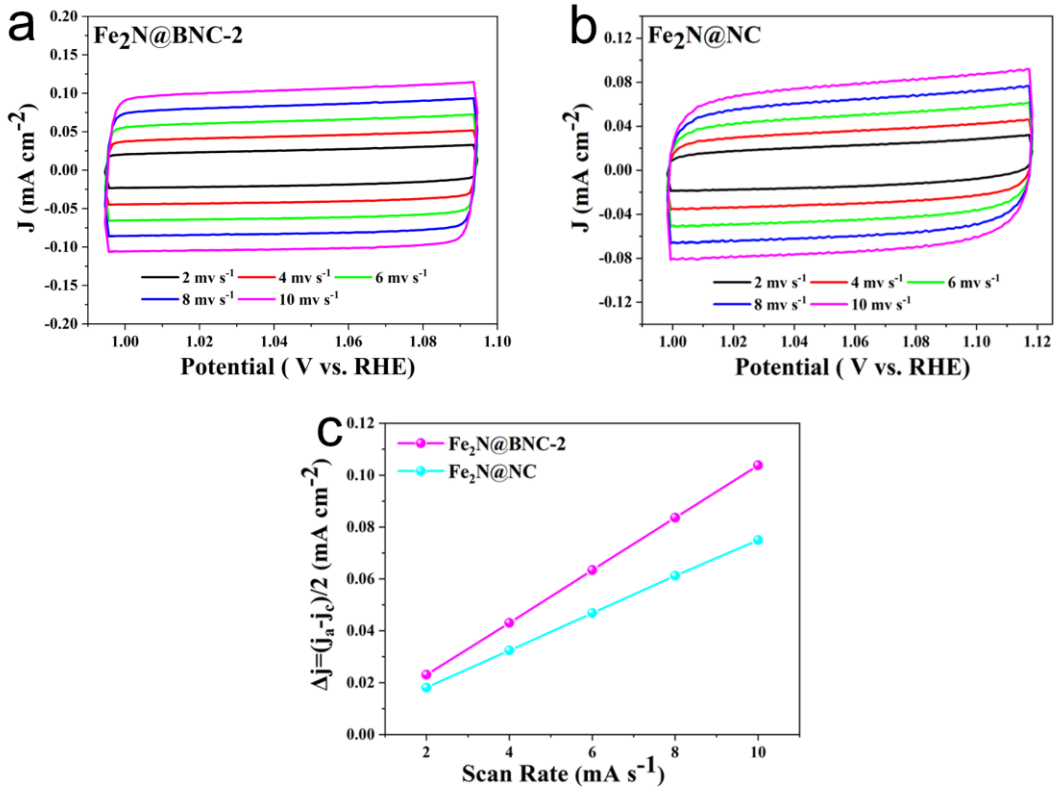

Fig. S13 (a, b) CV curves of Fe_2N@BNC-2 and Fe_2N@NC as a function of the pyrolysis temperature at various scan rates within a non-Faraday potential window (1 V-1.1 V). (c) Linear fitting of capacitive currents of catalysts vs. scan rate.

The electrochemical active surface area (ECSA) is determined via Formula (1), where the double layer capacitance (C_{dl}) value was estimated by the linear slope of the fitted line which was plotted by capacitive currents versus scan rates, and the C_s value is adopted as ≈0.04 mF cm^{-2}.

$$ECSA = \frac{C_{dl}}{C_s} \quad (1)$$

The ECSA of Fe_2N@BNC-2 and Fe_2N@NC is calculated to be 252.5 and 178.0 cm^2, respectively, further confirming the higher activity of Fe_2N@BNC-2.

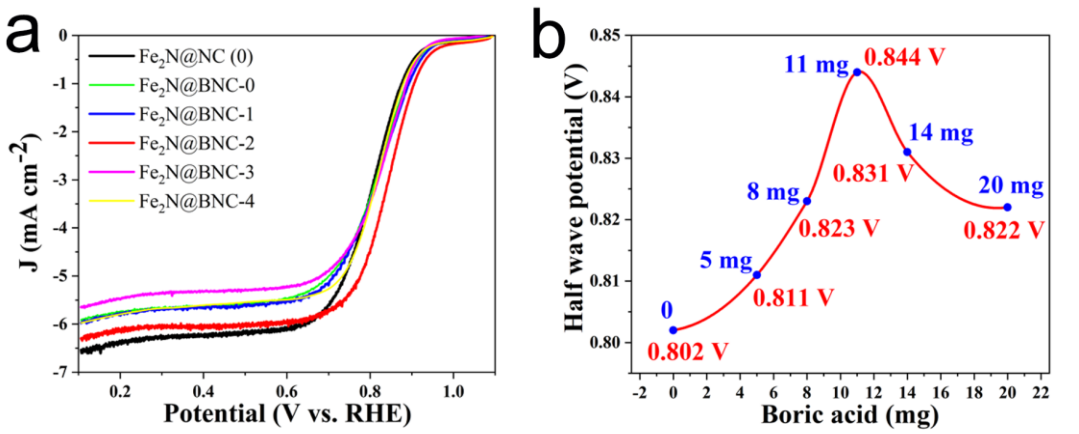

Fig. S14 (a) The polarization curves of Fe_2N@NC, Fe_2N@BNC-0, Fe_2N@BNC-1, Fe_2N@BNC-2, Fe_2N@BNC-3 and Fe_2N@BNC-4 loaded on GC in a O_2-saturated 0.1 M KOH solution at a 5 mV s^{-1} scan rate and a rotation rate of 1600 rpm. (b) Half-wave potential of catalysts with different boron precursor content, the corresponding relationship with Figure a is as follows: Fe_2N@NC (No boron), Fe_2N@BNC-0 (5 mg), Fe_2N@BNC-1 (8 mg), Fe_2N@BNC-2 (11 mg), Fe_2N@BNC-3 (14 mg), Fe_2N@BNC-4 (20 mg).

Half-wave potential of catalysts with different atomic ratio of boron, the corresponding relationship with Figure 3f are as follows: Fe_2N@NC (No boron), Fe_2N@BNC-1 (1.00 at %), Fe_2N@BNC-2 (1.22 at %), Fe_2N@BNC-3 (3.16 at %). N content of catalysts with different atomic ratio of boron, the corresponding relationship in Figure 3f are as follows: Fe_2N@NC (0.45 at %), Fe_2N@BNC-1 (1.33 at %), Fe_2N@BNC-2 (3.02 at %), Fe_2N@BNC-3 (2.78 at %). The relationship between C-N-B content in wrapped layer and atomic ratio of boron as follows: Fe_2N@NC (No C-N-B), Fe_2N@BNC-1 (30.1 %), Fe_2N@BNC-2 (35.3 %), Fe_2N@BNC-3 (26.1 %).

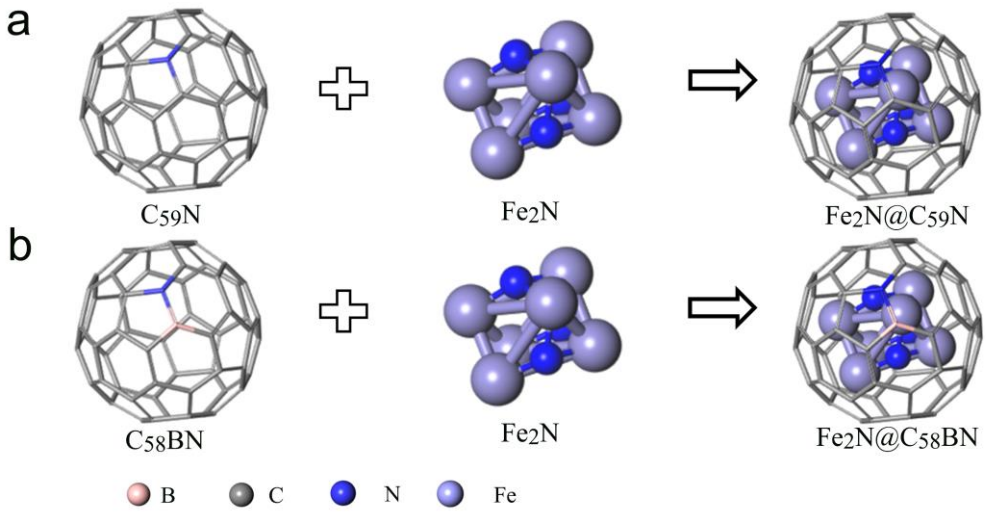

Fig. S15 The optimized structure of $Fe_2N@C_{59}N$ (a) and $Fe_2N@C_{58}BN$ (b).

As shown in the Fig. S15, we have constructed $Fe_2N@C_{59}N$ and $Fe_2N@C_{58}BN$ catalyst models based on C_{60} and Fe_2N clusters. After optimizing the structure, it was found that the shell of the catalyst did not undergo major structural changes, indicating that the constructed model was stable. The bond lengths between the C, B, N atoms in the $Fe_2N@C_{58}BN$ shell and the Fe atom in Fe_2N are 2.10, 2.05, and 1.98 Å, respectively. The bond lengths between C, N atoms in the shell of $Fe_2N@C_{59}N$ and Fe atoms in Fe_2N are 1.94 and 1.97 Å.

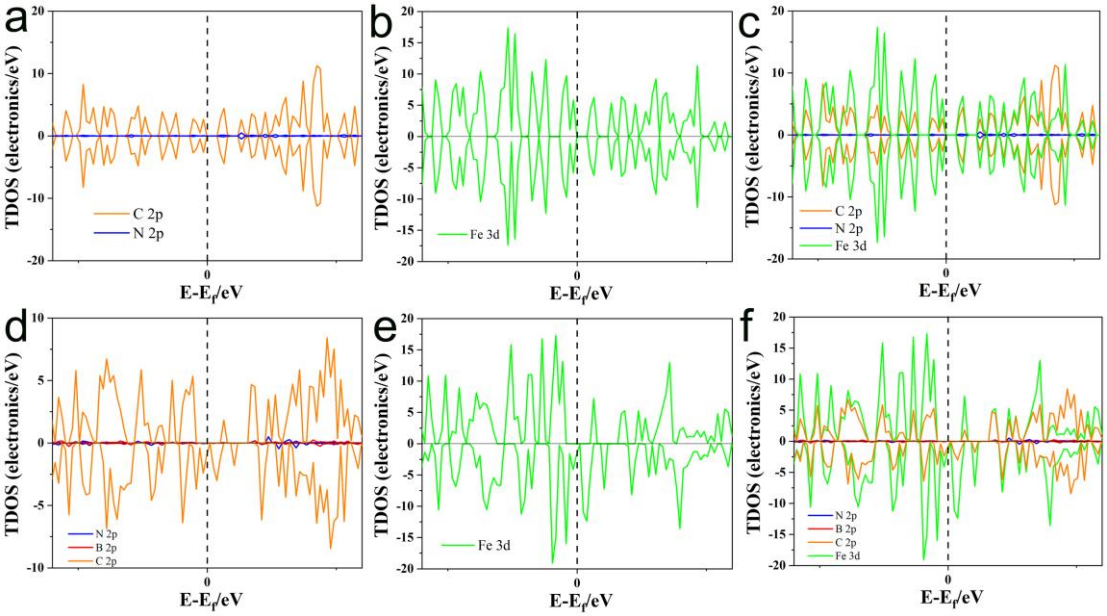

Fig. S16 The projected density of states of $Fe_2N@C_{59}N$ (a, b, c) and $Fe_2N@C_{58}BN$ (d, e, f).

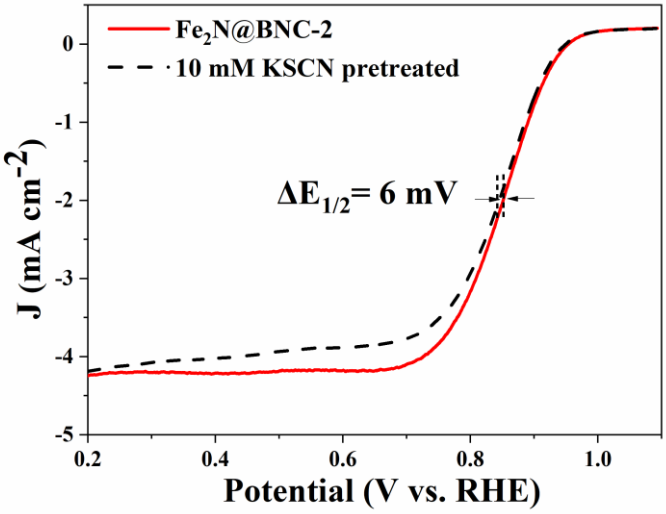

Fig. S17 Effect of SCN^- on the ORR activity of Fe_2N@BNC-2 in O_2-saturated 0.1 M KOH solution.

Table S1. The contents of Fe, C, O, N and B in samples.

Samples	XPS composition (at %)				
	Fe	C	O	N	B
Fe_2N@BNC-1	0.52	94.14	3.01	1.33	1.00
Fe_2N@BNC-2	0.38	92.75	2.63	3.02	1.22
Fe_2N@NC	0.97	95.06	3.15	0.82	-

Table S2. Comparison of various ORR electrocatalysts in alkaline solution.

Catalyst	Onset potential (V vs. RHE)	Half-wave potential (V vs. RHE)	Current density at 0.3 V ($mA \cdot cm^{-2}$)	Years	Ref.
Fe_2N@BNC-2	**0.981**	**0.844**	**6.06**	**This work**	**This work**
FeSe@NC-900 [1]	0.970	0.800	5.40	2021	J. Mater. Chem. A
Co/CoO@NSC [2]	0.975	0.835	5.50	2022	J. Energy Chem.
N-hG6 [3]	0.910	0.833	5.28	2020	Carbon
Fe_2N@NPC-500 [4]	0.927	0.790	4.85	2017	Nanoscale
Co–N/CNTs-900 [5]	0.908	0.784	5.66	2021	J. Energy Chem.
BN/C [6]	0.880	0.800	5.25	2020	Carbon
Fe_3C@C-900 [7]	0.910	0.800	5.28	2017	Carbon
BCN [8]	0.940	0.820	5.50	2017	ACS. Energy Lett.
Fe@C [9]	0.820	0.712	4.50	2016	J. Am. Chem. Soc.
CMN-231H [10]	0.945	0.780	5.80	2021	Chem. Eng. J.
Fe-Mn_3O_4 HYSNBs [11]	1.02	0.780	5.85	2022	Chem. Eng. J.
Fe_xN/NGA [12]	0.965	0.815	5.78	2014	Adv. Funct. Mater.
$Fe_{1-x}S$@NSC-24 [13]	0.980	0.700	5.05	2021	J. Energy Chem.
MnO@FLC [14]	0.935	0.813	5.38	2016	J. Mater. Chem. A
M_3C-GNRs [15]	0.950	0.820	4.60	2015	ACS Nano
Fe-N-C/HPC-NH_3 [16]	0.945	0.803	6.01	2019	Nano Research
Fe/N-CNTs [17]	0.960	0.810	5.05	2016	J. Mater. Chem. A
B_2NGFe_2-800 [18]	0.980	0.830	4.95	2016	Phys. Chem. Chem. Phys.

References

1. Y. Cao, S. Huang, Z. Peng, F. Yao, X. Li, Y. Liu, H. Huang and M. Wu, *J. Mater. Chem. A*, 2021, **9**, 3464-3471.
2. D. Zhou, H. Fu, J. Long, K. Shen and X. Gou, *J. Energy Chem.*, 2022, **64**, 385-394.
3. Y. Bian, H. Wang, J. Hu, B. Liu, D. Liu and L. Dai, *Carbon*, 2020, **162**, 66-73.
4. X. Huang, Z. Yang, B. Dong, Y. Wang, T. Tang and Y. Hou, *Nanoscale*, 2017, **9**, 8102-8106.
5. X. Wang, X. Xi, G. Huo, C. Xu, P. Sui, R. Feng, X.-Z. Fu and J.-L. Luo, *J. Energy Chem.*, 2021, **53**, 49-55.
6. R. Zhao, Q. Li, Z. Chen, V. Jose, X. Jiang, G. Fu, J.-M. Lee and S. Huang, *Carbon*, 2020, **164**, 398-406.
7. A. Kong, Y. Zhang, Z. Chen, A. Chen, C. Li, H. Wang and Y. Shan, *Carbon*, 2017, **116**, 606-614.
8. J. Wang, J. Hao, D. Liu, S. Qin, D. Portehault, Y. Li, Y. Chen and W. Lei, *ACS. Energy Lett.*, 2017, **2**, 306-312.
9. W. J. Jiang, L. Gu, L. Li, Y. Zhang, X. Zhang, L. J. Zhang, J. Q. Wang, J. S. Hu, Z. Wei and L. J. Wan, *J. Am. Chem. Soc.*, 2016, **138**, 3570-3578.
10. B. Chen, H. Miao, M. Yin, R. Hu, L. Xia, C. Zhang and J. Yuan, *Chem. Eng. J.*, 2021, **417**.
11. T. Li, Y. Hu, K. Liu, J. Yin, Y. Li, G. Fu, Y. Zhang and Y. Tang, *Chem. Eng. J.*, 2022, **427**.
12. H. Yin, C. Zhang, F. Liu and Y. Hou, *Adv. Funct. Mater.*, 2014, **24**, 2930-2937.
13. Z. Li, W. Wang, M. Zhou, B. He, W. Ren, L. Chen, W. Xu, Z. Hou and Y. Chen, *J. Energy Chem.*, 2021, **54**, 310-317.
14. H. Cheng, K. Xu, L. Xing, S. Liu, Y. Gong, L. Gu, L. Zhang and C. Wu, *J. Mater. Chem. A*, 2016, **4**, 11775-11781.
15. X. Fan, Z. Peng, R. Ye, H. Zhou and X. Guo, *ACS Nano*, 2015, **9**, 7407-7418.
16. X. Liu, H. Liu, C. Chen, L. Zou, Y. Li, Q. Zhang, B. Yang, Z. Zou and H. Yang, *Nano Research*, 2019, **12**, 1651-1657.
17. Y. Liu, H. Jiang, Y. Zhu, X. Yang and C. Li, *J. Mater. Chem. A*, 2016, **4**, 1694-1701.
18. H. Feng, L. Wang, L. Zhao, C. Tian, P. Yu and H. Fu, *Phys. Chem. Chem. Phys.*, 2016, **18**, 26572-26578.